Title

The Chronic Wound Phageome: Phage Diversity and Associations with Wounds and Healing Outcomes.

Journal

Microbiology Spectrum, 10(3)

Authors

Verbanic, Samuel

Deacon, John

Chen, Irene

Publication Date

2022-06-29

DOI

10.1128/spectrum.02777-21

Peer reviewed

AMERICAN SOCIETY FOR MICROBIOLOGY | Microbiology Spectrum

RESEARCH ARTICLE

The Chronic Wound Phageome: Phage Diversity and Associations with Wounds and Healing Outcomes

Samuel Verbanic,[a] John M. Deacon,[b] Irene A. Chen[a]

[a]Department of Chemical and Biomolecular Engineering, University of California, Los Angeles, California, USA
[b]Goleta Valley Cottage Hospital, Ridley-Tree Center for Wound Management, Santa Barbara, California, USA

ABSTRACT Two leading impediments to chronic wound healing are polymicrobial infection and biofilm formation. Recent studies have characterized the bacterial fraction of these microbiomes and have begun to elucidate compositional correlations to healing outcomes. However, the factors that drive compositional shifts are still being uncovered. The virome may play an important role in shaping bacterial community structure and function. Previous work on the skin virome determined that it was dominated by bacteriophages, viruses that infect bacteria. To characterize the virome, we enrolled 20 chronic wound patients presenting at an outpatient wound care clinic in a microbiome survey, collecting swab samples from healthy skin and chronic wounds (diabetic, venous, arterial, or pressure) before and after a single, sharp debridement procedure. We investigated the virome using a virus-like particle enrichment procedure, shotgun metagenomic sequencing, and a *k*-mer-based, reference-dependent taxonomic classification method. Taxonomic composition, diversity, and associations with covariates are presented. We find that the wound virome is highly diverse, with many phages targeting known pathogens, and may influence bacterial community composition and functionality in ways that impact healing outcomes.

IMPORTANCE Chronic wounds are an increasing medical burden. These wounds are known to be rich in microbial content, including both bacteria and bacterial viruses (phages). The viruses may play an important role in shaping bacterial community structure and function. We analyzed the virome and bacterial composition of 20 patients with chronic wounds. The viruses found in wounds are highly diverse compared to normal skin, unlike the bacterial composition, where diversity is decreased. These data represent an initial look at this relatively understudied component of the chronic wound microbiome and may help inform future phage-based interventions.

KEYWORDS chronic wound, microbiome, phageome, virome

Chronic wounds (i.e., those that fail to exhibit reasonable healing progress within an expected time frame) are a growing source of morbidity and mortality worldwide (1–3). While not always infected, chronic wounds are frequently colonized by polymicrobial communities. Characterization of these communities is important for understanding the microbial content of wounds and the potential influence of the wound microbiome on healing outcomes. Recently, several culture-independent studies have characterized the extensive microbial diversity of skin and wounds (4–25). These studies have found that wound communities are primarily composed of *Staphylococcus* spp., *Pseudomonas* spp., *Corynebacterium* spp., *Streptococcus* spp., *Anaerococcus* spp., and *Enterococcus* spp., and numerous low-abundance taxa. However, significant interpatient variability in the composition of the wound microbiome exists, which cannot be explained by covariates like age, race, sex, or wound etiology (9, 11). Still, some studies have indicated that community composition may be associated with healing

Editor David T. Pride, University of California, San Diego

Address correspondence to Irene A. Chen, ireneachen@ucla.edu.

The authors declare no conflict of interest.

Received 29 December 2021
Accepted 12 March 2022
Published 18 April 2022

outcomes. Temporal instability and the transition between several distinct community structures were associated with positive healing outcomes (4), and communities with high proportions of aerobes and facultative anaerobes were associated with poor healing outcomes (26).

While the bacterial content of chronic wounds has been the subject of substantial study, the wound virome has received less attention. Previous works have determined that the human virome is mostly composed of bacteriophages, the viruses that infect bacteria (27, 28). The ability of bacteriophages to infect, kill, and modulate bacterial host function has been well described (29–31), and the wound virome may therefore represent a previously understudied explanatory variable for interpatient variability, healing outcomes, community dynamics, and pathogenicity (28, 32–34). Despite its potentially influential role in the bacterial microbiome, studies of the virome are often hindered by insufficient sequencing depths. Although viruses and phages are highly abundant in number (outnumbering bacterial cells approximately 10:1) (29), their typically small genome sizes result in a small fractional abundance of viral DNA sequences compared to prokaryotic and eukaryotic DNA. Therefore, virus-like particle (VLP) enrichment is necessary to obtain substantial sequencing depth of the viral fraction. VLP enrichment does have limitations, though. These methods capture free particles and therefore do not detect latent viruses (e.g., lysogenic phages) or their replicative intermediates inside intact cells. Additionally, depending on the methods used, certain classes of viruses may not be detected. In particular, the methods used in this work were designed to detect double-stranded DNA (dsDNA) and single-stranded DNA (ssDNA) viruses but are not suitable for RNA viruses.

The viral fraction of the healthy skin microbiome has been studied (35, 36), but to date, only one study has employed a VLP enrichment method (37). In this study, 91% of putative viral contigs for dsDNA viruses could not be taxonomically classified; among those that could be classified, most belonged to the order *Caudovirales* and targeted *Staphylococcus* spp., *Corynebacterium* spp., *Streptococcus* spp., *Propionibacterium* spp., and *Pseudomonas* spp., and the most common virus infecting humans was papillomavirus. Virome composition and diversity were associated with the skin site (e.g., sebaceous or moist, occluded or exposed), and exhibited high intrapersonal variance but less temporal variance at a given site. Despite progress in describing the human virome in general (27, 28, 38), no studies have used VLP enrichment methods and metagenomics to characterize the wound virome. The phage content of chronic wounds is of particular interest, as long-term community dynamics, which may be influenced by phages, might affect healing outcomes (4, 26).

Here, we characterize the chronic wound viromes of 20 patients presenting to an outpatient wound care clinic. Swabs were collected from chronic wounds before and after a single, sharp debridement event, along with a skin sample from the contralateral limb (abbreviated as "cl. skin" below). For a detailed description of the patient cohort, see reference 26. We previously reported characterization of the bacterial communities by Illumina sequencing of the V1-V3 loops of the 16S rRNA genes (26), including the finding that facultative anaerobes, particularly *Enterobacter*, were significantly associated with nonhealing wounds. In the present work, we characterize the viral fraction of these samples. Samples were fractionated to enrich for VLPs while retaining a separate bacterial fraction, as described in reference 39. The VLP fraction was characterized by shotgun sequencing, with read classification and taxonomic abundance analysis performed with Kraken2 and Bracken, respectively, using a custom database containing the latest NCBI Viral RefSeq genomes and the Joint Genome Institute's IMG/VR viral metagenome database (40–43). Viromes were analyzed using ecological diversity metrics and differential abundance analyses. We report the composition of dsDNA viromes from the chronic wounds as well as the contralateral skin sites and find that wounds harbor significantly more diverse viral communities than cl. skin, with most viruses being bacteriophages. Additionally, we identify specific taxonomic associations with wounds compared to cl. skin and for healing outcomes (healed versus unhealed

wounds). This study thus reports an investigation of the previously uncharacterized chronic wound virome.

RESULTS

Read processing and classification. High-throughput sequencing of DNA from virus-like particles (VLPs) isolated from cl. skin and wound samples, along with negative controls, resulted in 635,166,925 total paired-end reads (9,623,741 ± 5,091,161 per sample, on average). Reads were quality and adapter trimmed, length-filtered, and joined, resulting in 556,645,739 preprocessed reads (8,434,026 ± 4,541,820 per sample, on average), which equates to an overall read retention rate of 86.64% (87.49% ± 9.92% per sample, on average). An initial assessment of overall taxonomic composition against the full NCBI RefSeq database indicated that most sequences had human or bacterial origin, though viral read abundances were still substantial (see Fig. S1 in the supplemental material).

To better assess the viral content of the samples, reads were reclassified with Kraken2 against the NCBI Viral RefSeq database, followed by classification against JGI's IMG/VR database, a large, public viral metagenome repository (42, 43). Taxon abundance estimates were again calculated with Bracken. Using this method, viral read classification was 379,992 ± 581,996 viral reads per sample, on average. Two types of taxonomic classifications were assigned to each hit: a viral species designation as assigned by NCBI or IMG/VR, if available, and a viral "type" designation, which denotes host association for prokaryotic viruses or common viral family name for eukaryotic viruses. For phages, the viral type designation is also referred to in the report below as the presumed host species. Additional information regarding the curation of taxonomic designations can be found in Materials and Methods.

To identify likely contaminants, negative-control samples were prepared and sequenced in parallel with the true samples. At the "type" level, *Escherichia* phage and unclassified viruses were found to be potential contaminants (Fig. S2a), possibly due in part to experiments carried out in adjacent lab spaces. In the negative controls, at the species level, ambiguous *Escherichia* phage and unclassified taxa were the most abundant, followed by known lab strains including *Escherichia* viruses Lambda, DE3, T7, T4, and M13 (Fig. S2b). An initial decontamination procedure was implemented with the R package Decontam, which identifies taxa that are more prevalent in negative controls than true samples (44). Using the four sequenced negative-control samples and a stringent threshold for declaring a contaminant, Decontam identified 39 potential contaminants. In addition, taxa corresponding to known lab strains were manually removed (Fig. S3 and S4).

After decontamination, most of the virome could be assigned as a species or to a host organism. Nevertheless, many taxa had no known host association, accounting for 42.27% ± 18.72% average relative abundance (Fig. S5). Unless otherwise stated, the following results focus on the "defined" fraction of the virome, which has viral species designation and/or "type"-level assignment of host species.

Abundant viral species and phage hosts in skin and wound viromes. Skin samples collected from the contralateral limb (cl. skin) exhibited high relative abundance of phages presumed to infect *Chryseobacterium*, *Neisseria*, *Staphylococcus*, *Yersinia*, *Bacillus*, *Pseudomonas*, *Salmonella*, *Corynebacterium*, and *Streptococcus* (Fig. 1). Accordingly, the most abundant identifiable viral species on cl. skin were unnamed *Neisseria*, *Yersinia*, *Bacillus*, *Corynebacterium*, *Streptococcus*, and *Pseudomonas* phages (Fig. S6). Among viruses that infect humans, papillomavirus was the most common.

Within the wound samples, the most prominent presumed phage hosts were *Proteus*, *Actinobaculum*, *Staphylococcus*, *Campylobacter*, *Yersinia*, *Pseudomonas*, and *Salmonella* (Fig. 1). For viruses that could be identified at the species level, wounds had high abundances of *Proteus* phage VB PmiS, an unnamed *Actinobaculum* phage, *Pseudomonas* virus phiCTX, and *Staphylococcus* phages StauST398-5 and Sextaec (Fig. S6). The top viral types shared between cl. skin and wounds are presumed to infect *Staphylococcus*, *Yersinia*, *Pseudomonas*, and *Salmonella*.

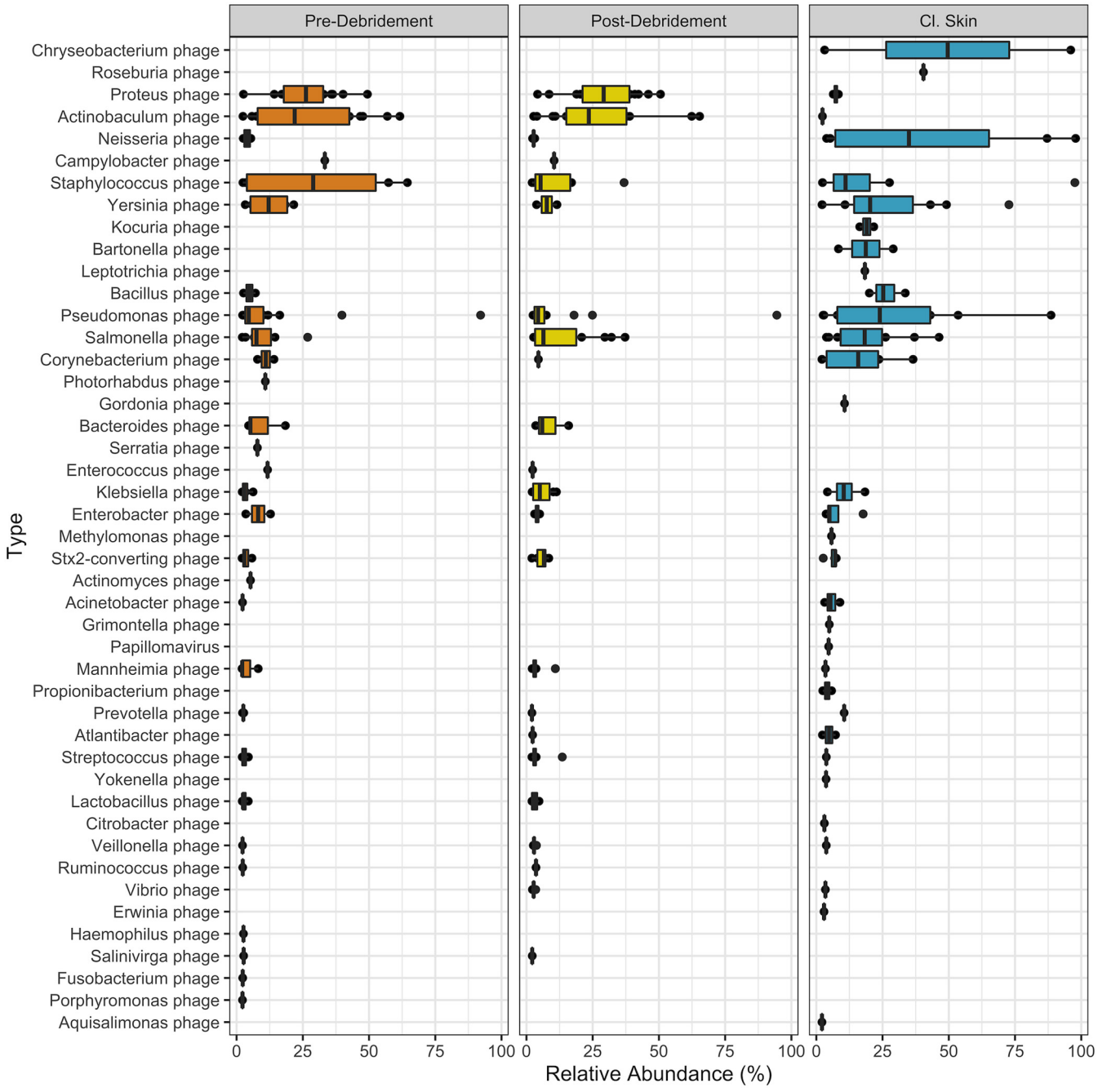

FIG 1 Taxonomic composition of viruses identified in wound (predebridement and postdebridement) and cl. skin samples. Relative abundance is given for each taxon of >2% at the "type" level (presumed host designation). Center line, median; box limits, upper and lower quartiles; whiskers, 1.5× interquartile range; points, outliers; $n = 20$ patients.

Viral diversity is greater in wounds than in skin. The virome exhibits significantly higher intrasample taxonomic richness and evenness in wounds than cl. skin, as measured by alpha diversity metrics with unclassified taxa included (Fig. 2a). In terms of richness, wounds had an average Chao1 index of 996 ± 426 while cl. skin had an average of 101 ± 271. Accounting for abundance and evenness, wounds had an average Shannon index of 4.70 ± 0.72 while cl. skin had an average of 1.95 ± 1.23. The differences in richness and evenness can be qualitatively visualized in a relative abundance heatmap of the top 300 taxa (Fig. 2b). The findings contrast with diversity of the bacterial fraction of skin and wound microbiomes, in which bacterial diversity is consistently higher in normal skin than in wounds (26) (Fig. 2c). To eliminate the possibility that

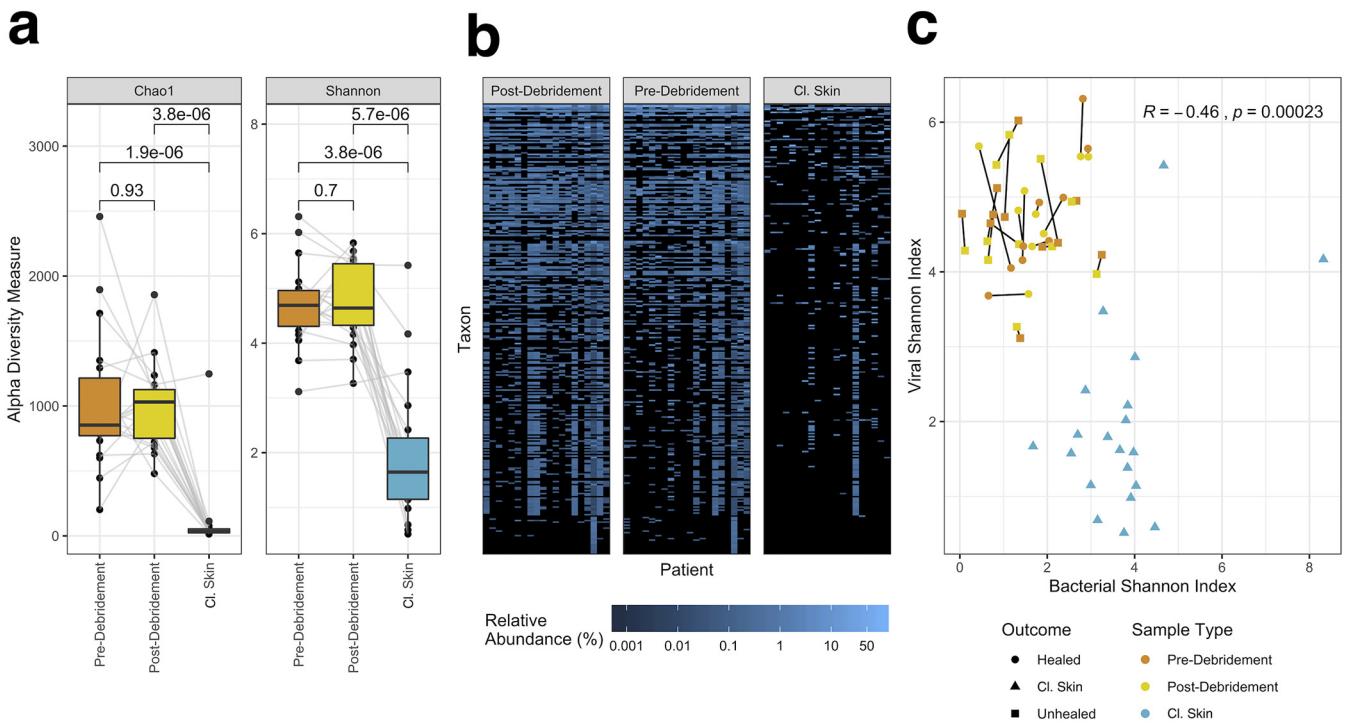

FIG 2 Alpha diversity of cl. skin and wound viromes. (a) Boxplots of Chao1 and Shannon indices in wound samples (pre- and postdebridement) and cl. skin samples, with each patient's samples connected by gray lines. Center line, median; box limits, upper and lower quartiles; whiskers, 1.5× interquartile range; points, outliers; $n = 20$ patients. Averages were compared with paired, two-sided Wilcoxon signed-rank tests, resulting in the P values shown. (b) Heatmap of relative abundance of the top 300 taxa in each patient's pre-/postdebridement and cl. skin samples. For figure labels, see the spreadsheet in the supplemental material. (c) Correlation between viral and bacterial Shannon indices, with pre- and postdebridement samples from the same wound connected by a black line, sample type indicated by color, and outcome indicated by shape. Pearson's correlation coefficient R and P value are shown, calculated using all samples.

increased richness was due to greater sampling, we subsampled each sample to an equal depth and performed the same diversity analysis. The trends in phage diversity remained the same (higher diversity in wounds than in cl. skin) (Fig. S7), indicating that the differences were not driven by sample size.

Skin and wound viromes are taxonomically distinct. Diversity between samples (beta diversity) was measured using Bray-Curtis distance and visualized by principal-coordinate analysis. Unclassified taxa were included. Cl. skin and wound samples partitioned well from each other (Fig. 3a), indicating that they harbor distinct viromes. As observed previously for the bacterial fraction, pre- and postdebridement wound samples were more similar to each other than to the corresponding cl. skin sample (Fig. 3b).

Specific viral species and hosts associated with skin and wound samples. Species associations with cl. skin and wound sample types were also explored by differential abundance analysis using DESeq2. Although unique phage species were associated with each sample type, the hosts they targeted were largely shared, including *Yersinia* spp., *Neisseria* spp., *Pseudomonas* spp., *Streptococcus* spp., *Salmonella* spp., and *Staphylococcus* spp. (Fig. 4). Nevertheless, cl. skin and wounds differed in some of the host species targeted. Cl. skin was associated with one *Staphylococcus haemolyticus* phage, one *Staphylococcus aureus* phage, and two general *Pseudomonas* phages, while wounds had many associations with *Staphylococcus aureus* and *Pseudomonas formosensis* phage species.

Viral species associated with healing outcomes. To identify specific taxonomic associations with covariates, differential abundance analysis was performed with DESeq2 (Fig. 5). Wound were classified according to whether they healed within 6 months after sampling. Within wound samples, associations with healing outcomes are of primary interest. After filtering the results to retain associations with adjusted P values of <0.01, both healed and unhealed wounds were found to be associated with

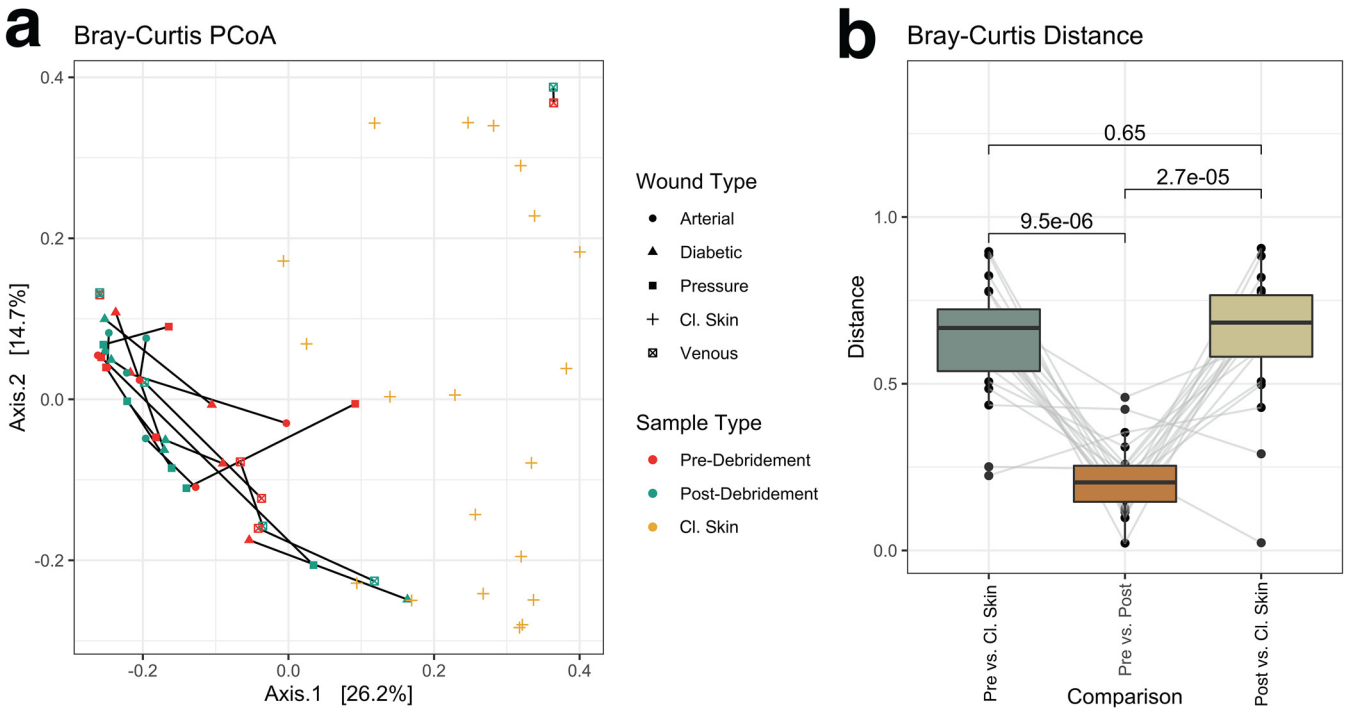

FIG 3 Beta diversity as measured by Bray-Curtis dissimilarity. Taxa present in >2 samples with >0.5% relative abundance (including unclassified taxa) were retained for analysis. Ordination of the Bray-Curtis dissimilarity matrix using principal-coordinate analysis (PCoA) (a) illustrates distinct compositions for wound and cl. skin samples. Within-patient dissimilarity between predebridement, postdebridement, and cl. skin samples with averages was compared by two-sided Wilcoxon signed-rank tests (*P* values shown), and data from each patient are connected by gray lines (b). Center line, median; box limits, upper and lower quartiles; whiskers, 1.5× interquartile range; points, outliers; $n = 20$ patients.

specific *Staphylococcus* phage. Healed wounds were also associated with many *Pseudomonas*, *Campylobacter*, and *Bacteroides* phage, while unhealed wounds were associated with *Enterococcus*, *Enterobacter*, *Veillonella*, and *Streptococcus* phage. Host association was known for these phages, but most did not have species designations approved by the International Committee on Taxonomy of Viruses (ICTV).

DISCUSSION

Using deep sequencing, we characterized the cl. skin and chronic wound viromes of 20 patients presenting at a wound care clinic. Samples were processed using a virus-like particle (VLP) enrichment protocol to capture actively replicating viruses, reduce host contamination, and increase viral sequencing depth. Here, we report the taxonomic composition of the viromes, associated ecological diversity measures, and specific taxa associated with healing outcomes and sample types.

Host contamination was assessed by classifying reads against the full NCBI RefSeq database, indicating a high abundance of human and bacterial DNA. It should be noted that this assessment underestimates true viral read abundances, which may be aligned with CRISPR spacers and prophages in bacterial reference genomes (45, 46). Additionally, since NCBI's viral reference database is incomplete, unclassified reads may have viral origin. Despite the implementation of VLP enrichment procedures and attempted depletion of host DNA, the prevalence of human and bacterial contamination underscores the need for extensive host DNA degradation during sample processing.

Viral detection and classification were performed with unassembled reads in a *k*-mer-based, reference-dependent manner. A viral metagenome database was utilized to capture relatively new or poorly annotated viruses. Nevertheless, approximately half of viral taxa detected had no known host or species annotation, similar to previous work in the field (37, 47). These results are consistent with a large, unclassified fraction of viral material, emphasizing the importance of read assembly, protein homology searches, and other methods for characterizing the virome (45, 48–52). Regardless, of

FIG 4 Differential abundance analysis of cl. skin and chronic wound viromes with DESeq2. Associated species are represented by their log2FoldChange from the normalized, geometric mean calculated across all wound samples, contrasting cl. skin (negative change) with wounds (positive change). Error bars represent the log-fold standard error; $n = 20$ patients. Only species with adjusted P values of <0.05 are shown. Relative abundance of each associated species, in each sample, is shown on the right; wound samples (predebridement) are red, and cl. skin samples are blue.

the annotated viral taxa, most targeted abundant cl. skin and wound bacteria such as *Proteus* spp., *Actinobacteria.*, *Pseudomonas* spp., *Staphylococcus* spp., *Corynebacterium* spp., *Streptococcus* spp., and mixed *Proteobacteria*. Wound samples tended to contain pathogen-targeting phages, while cl. skin samples were associated with phages targeting commensals, consistent with the bacterial taxa present in the respective sample types previously detected using 16S rRNA sequencing (26).

Diversity analysis, including the unannotated viral taxa, showed that wound viromes were significantly more diverse than cl. skin viromes in both taxonomic richness and evenness. Interestingly, viral diversity was negatively correlated with bacterial diversity. This correlation did not appear to be an artifact of low viral sampling depth of cl. skin, since subsampling to the same depth gave similar results (see Fig. S7 in the supplemental material). The findings suggest that the wound environment, while resulting in low bacterial diversity, may be hospitable to proliferation of diverse

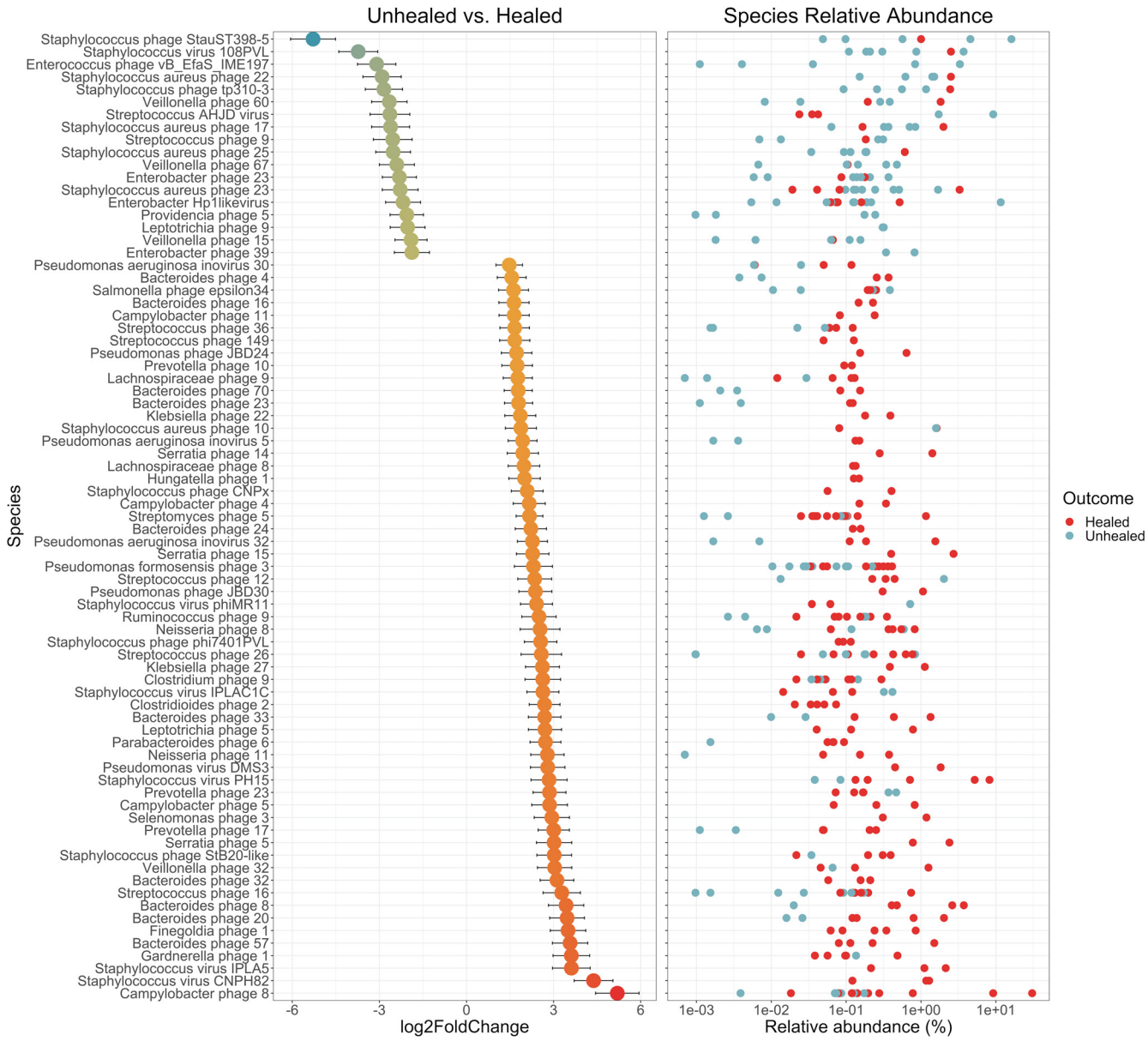

FIG 5 Differential abundance analysis of healed and unhealed wound viromes with DESeq2. Associated species are represented by their log2FoldChange from the normalized, geometric mean calculated across all wound samples, contrasting unhealed (negative change) with healed (positive change) wounds. Error bars represent the log-fold standard error; $n = 20$ patients. Only species with adjusted P values of <0.01 are shown. Relative abundance of each associated species, in each sample, is shown on the right; healed wound samples are red, and unhealed wound samples are blue. Numeric species designations given were assigned by this study.

phages. Wound treatment may also encourage phage proliferation, as lysogenic phage may switch to the lytic life cycle in response to antibiotics (53), reactive oxygen species (54), DNA damage signaled by SOS responses (55), and various stress responses to changes in the environment, like pH (56, 57). Cl. skin and wound viromes were also nonlinearly partitioned by beta diversity ordination, illustrating that their compositions were distinct.

To characterize possible taxonomic associations with wound healing status, wounds were classified as healed (8 wounds) or unhealed (12 wounds), based on whether the wound had healed within 6 months after sampling. Differences between the viromes of healed and unhealed wounds were characterized by differential abundance analysis. Several significantly associated taxa displayed unique functional properties that could influence healing outcomes (Table 1). Both healed and unhealed wounds were largely

TABLE 1 Traits of viruses associated with healed and unhealed wounds

Association	Species	Known host(s)	Life cycle	Notable trait(s)	Reference
Healed	*Pseudomonas* phage JBD24	*Pseudomonas aeruginosa*	Temperate	Inhibits motility (equivalent to pilus knockout); reduced biofilm formation	61
Healed	*Pseudomonas* phage JBD30	*Pseudomonas aeruginosa*	Temperate	Inhibits CRISPR systems	63
Healed	*Pseudomonas* phage DMS3	*Pseudomonas aeruginosa*	Temperate	Inhibits biofilm formation; exhibits CRISPR resistance	62
Healed	*Salmonella* phage epsilon34	*Salmonella enterica* subsp. *enterica* serovar	Temperate	P22/lambdoid phage (potential contaminant); alters *Salmonella* serotype	83
Healed	*Staphylococcus* phage CNPx	*Staphylococcus epidermidis*	Temperate		84
Healed	*Staphylococcus* phage phi7401PVL	*Staphylococcus aureus*	Temperate	Carries pore-forming toxin PVL	58
Healed	*Staphylococcus* phage StB20-like	*Staphylococcus epidermidis*; *Staphylococcus hominis*	Temperate		85
Healed	*Staphylococcus* phage CNPH82	*Staphylococcus epidermidis*	Temperate		86
Healed	*Staphylococcus* phage IPLA5	*Staphylococcus epidermidis*	Lytic	Pectin lyase-like domains; antibiofilm activity	64
Healed	*Staphylococcus* phage IPLAC1C	*Staphylococcus* subspecies	Lytic		87
Healed	*Staphylococcus* phage PH15	*Staphylococcus epidermidis*	Temperate		86
Healed	*Staphylococcus* phage phiMR11	*Staphylococcus aureus*	Temperate		88
Unhealed	*Enterobacter* Hp1likevirus	*Enterobacter*	Lytic		89
Unhealed	*Enterococcus* phage vB_EfaS_IME197	*Enterococcus faecalis*	Temperate		90
Unhealed	*Staphylococcus* phage tp310-3	*Staphylococcus aureus*	Temperate		91
Unhealed	*Staphylococcus* phage108PVL	*Staphylococcus aureus*	Temperate	Carries pore-forming toxin PVL	59
Unhealed	*Staphylococcus* phage StauST398-5	*Staphylococcus aureus*	Temperate		92
Unhealed	*Streptococcus* phage AHJD	Group C streptococci	Lytic		93

associated with temperate phage in the family *Siphoviridae*, including *Staphylococcus* phages carrying Panton-Valentine leukocidin (PVL) genes (58, 59). Their presence in wounds may indicate a shift to the lytic cycle in the wound environment. Furthermore, as temperate phages, *Siphoviridae* may exert influence over their hosts' function through prophage integration and lysogenic conversion (31, 60). Of the lytic phages, healed wounds were associated with two *Staphylococcus* phage species, and unhealed wounds were associated with *Streptococcus* and putative *Enterobacter* phage species. Phage species associated with healed wounds may have profound impacts on host function, including reduction or inhibition of biofilm formation (61, 62), motility inhibition equivalent to a pilus knockout (61), CRISPR resistance or inhibition (62, 63), and antibiofilm activity via capsid-displayed pectin lyase-like domains (64). Biofilms are a leading impediment to wound healing, and exploitation of phage or their proteins as antibiofilm agents is a very active area of research (34, 65–67). Suppression of the CRISPR system might confer an advantage to the phage in evading degradation by the host. Recent work suggests that anti-CRISPR systems are dependent on multiplicity of infection, requiring several phage to be expressing the gene simultaneously in a rare case of interphage cooperation and altruism (68). The association of phages bearing such traits with healing of chronic wounds may warrant further investigation.

Both healed and unhealed wounds were associated with phage known to transduce the pore-forming toxin Panton-Valentine leukocidin (PVL), which may increase pathogenicity of their hosts by evading immune response and lysing leukocytes, though the specific role of leukocidins in wound pathogenesis is still unclear (69). The *Proteus* phage vB PmiS-TH was also prominent among wound samples. This *Siphoviridae* phage has been found to be lytic against *Proteus mirabilis*, a known wound pathogen, and may be a common wound commensal phage (70). Future studies would be needed to characterize any such possible functional associations.

Several considerations limit the analysis presented here. The protocols used here

are appropriate for nonenveloped dsDNA viral particles, possibly including replicative intermediates of ssDNA viruses. Other viruses, including prophages and RNA viruses, would require further investigation. We determined viral abundance and taxonomy using a *k*-mer-based approach at the nucleotide sequence level with unassembled reads. Read-based approaches can lead to false positives due to the short length of reads. Although Kraken2 has a relatively low false-positive rate compared to other tools (71), assembly into contigs and contig classification would likely be more accurate. Viral detection, taxonomic classification, and associations were therefore limited by existing reference databases. The NCBI Viral RefSeq database is relatively small but curated and annotated, while IMG/VR is large but less annotated. In particular, temperate bacteriophage may excise portions of the host genome when entering the lytic life cycle (31, 57); if such bacterial sequences were present in the IMG/VR database, bacterial contaminants in the sample data may have appeared as false-positive viral hits. In addition to this, the sequences contained a substantial amount of human and bacterial DNA despite the use of viral enrichment protocols, and *in silico* decontamination was needed. Contamination is a common issue for viral metagenomics, especially when working with low-biomass clinical samples (72, 73). Contamination was more prevalent for cl. skin samples, as expected given the lower DNA yields. Additional measures, such as more robust nuclease treatment and improved *in silico* decontamination methods, could improve sequence quality in future work. It should be noted that the samples were taken from wounds having different etiologies (diabetic, venous, arterial, or pressure), which may contribute to the high phage diversity observed. However, due to the small sample size, significant differences among these etiologies would be difficult to support statistically (Fig. S8). At the same time, a larger study previously showed no correlation between bacterial community composition and wound etiology (26). Finally, due to the small cohort size, only associations of relatively large effect could be detected, and the findings of this study should ideally be validated with larger cohorts.

Conclusion. Chronic wounds are frequently colonized and infected by polymicrobial communities, impeding wound healing. Previous work has established that the bacterial fraction of these communities exhibits high interpersonal variance, and community structure and function may be associated with healing outcomes. Yet the forces that drive compositional and functional dynamics of wound microbiomes have yet to be elucidated. We sought to better understand the role of a potentially important contributing factor, the virome. This study presents the first characterization of the chronic wound virome, utilizing a virus-like particle enrichment protocol and shotgun metagenomics to survey the wounds of 20 patients presenting at an outpatient wound care clinic. Despite heavy host contamination, we describe viral taxonomic composition, diversity, associations with covariates, and virus-host correlations.

While no causative or conclusive claims can be made regarding the virome's role in wound pathology, the rich inter- and intrapersonal taxonomic diversity and associations with covariates suggest that the virome is a prominent component of the greater microbiome and merits thorough investigation in the future. To achieve more sensitive viral detection and accurate taxonomic classification, future studies would benefit from shotgun sequencing both the bacterial and viral fractions of the microbiome, and assembling the resulting reads into contiguous sequences, which will facilitate protein homology searches and within-sample CRISPR spacer and prophage alignments. Furthermore, time series data will be imperative for elucidating the multitude of complex, dynamic bacterium-bacteriophage interactions. Such work will contribute to the greater understanding of how the wound microbiome as a whole is related to wound pathology and, ultimately, how it may be leveraged to achieve more positive healing outcomes.

MATERIALS AND METHODS

Ethics statement. Clinical sample collection was performed at the Ridley-Tree Center for Wound Management at Goleta Valley Cottage Hospital in accordance with protocols approved by the Cottage Health Institutional Review Board (study protocol 17-48u) and UCSB's Human Subjects Committee and

Institutional Review Board (study protocol 4-18-0190). A cohort of 20 wound care patients were recruited over the course of a week and a half, and samples were collected after obtaining informed, written consent from the patient.

Clinical sample collection. Samples were collected as previously described (26). Four clinically classified chronic wound types were sampled (diabetic ulcers, venous wounds, arterial wounds, and pressure ulcers), with five patients per wound type. Inclusion criteria were patients over the age of 18, presenting a clinically classified chronic wound for care with debridement. Exclusion criteria were patients under the age of 18, in the intensive care unit, or presenting with an infection in another part of the body (not related to the wound). All patients underwent nonconservative sharp debridement until bleeding was observed. However, the extent and depth of debridement, as well as the type of instrument (curette, scalpel, scissors, or tissue nipper), were not standardized and were determined by the treating physician (see reference 26). Sterile Copan FLOQSwabs 520C were prewetted with sterile phosphate-buffered saline (PBS) prior to all sample collections. During a single patient visit, wound swabs were collected predebridement and 1 to 2 min postdebridement, and a healthy skin swab was collected from the contralateral limb. Wound samples were collected from the area of debridement. All cl. skin and wound samples were collected by employing Levine's technique; gentle pressure was applied as the swab was wiped and rolled across a $\sim$1-cm^2 area of healthy granulation tissue for approximately 30 s. Clinical swabs were placed back into the dry, sterile collection tube and stored at 4°C for no more than 4 h before being processed. Negative-control samples from the wound center were collected by exposing swabs to air in the collection room for the same duration as wound and cl. skin swab collection. Processing control samples were obtained by exposing swabs to air and reagents in the processing lab analogously to clinical samples.

Sample processing and DNA extraction. Samples were processed as described previously (39). Briefly, swab tips were inserted into 1.5-mL microcentrifuge tubes and snapped at the 30-mm breakpoint. Five hundred microliters of sterile 1$\times$ Tris-EDTA (TE) was added to the tube, and the tube was vortexed for 2 min at maximum speed on a multitube vortex adapter to resuspend the sample. Samples were then centrifuged at 16,000 $\times$ *g* for 2 min to pellet cells. Two hundred fifty microliters of supernatant was transferred to a 2-mL microcentrifuge tube for immediate VLP precipitation. The remaining 250 μL of supernatant, pelleted cells, and swab tip was kept in the original tube and stored at $-$20°C before proceeding to whole-microbiome DNA extraction.

Isolation of DNA from virus-like particles. VLP purification and DNA extraction were conducted as described previously (39). Briefly, free DNA in the VLP fraction was digested with DNase I (5 units, New England Biolabs [NEB]; 2.5 μL) at 37°C for 30 min; DNase I was inactivated by incubation at 75°C for 10 min. VLPs were precipitated by adding 25 μL sterile 1$\times$ TE (pH 8.0), 2.5 μL 0.5 M EDTA (pH 8.0), 250 μL formamide, 7 μL GlycoBlue (15 mg/mL), and 1.1 mL 100% ethanol, followed by incubation at $-$20°C for 1 h and centrifugation for 1 h at $>$10,000 $\times$ *g* at 4°C. Pellets were washed with 500 μL of ice-cold 70% ethanol and repelleted by centrifugation for 30 min at $>$10,000 $\times$ *g* at 4°C. Pellets were dried for 1 h at room temperature in a Vacufuge before being resuspended in 152 μL sterile 1$\times$ TE (pH 8.0). Viral capsids were disrupted and digested with 10% SDS (final concentration of 1% [wt/vol]) and proteinase K (final concentration of 2.2 mg/mL), incubated at 55°C for 1 h. VLPs were further disrupted with 5 M NaCl and cetyltrimethylammonium bromide (CTAB)-NaCl, followed by incubation at 65°C for 10 min. The samples were then transferred to a phase lock gel tube (5Prime PLG Light) and mixed with 250 μL of 25:24:1 phenol-chloroform-isoamyl alcohol by inversion. Phases were separated by centrifugation at 1,500 $\times$ *g* for 5 min. In the same tube, 24:1 chloroform-isoamyl alcohol extraction was performed twice and the mixture was centrifuged as described above, and the 250-μL aqueous phase was transferred to a 2-mL microcentrifuge tube. DNA was purified by ethanol precipitation. Pellets containing DNA were washed with 500 μL ice-cold 70% ethanol, repelleted by centrifugation, and then dried for 1 h at room temperature in a Vacufuge and resuspended in 20 μL 1$\times$ TE (pH 8.0). The resulting final DNA concentration ranged from 0.01 to 12.9 ng/μL (mean = 1.28 ng/μL; median = 0.48 ng/μL), and the total DNA yield ranged from 0.2 to 258 ng (mean = 25 ng; median = 9.64 ng).

Library preparation and sequencing of VLP DNA. DNA from VLP-enriched samples was quantified using the Qubit dsDNA HS kit. Two library preparation methods were utilized depending on DNA concentration. Both methods are based on the Nextera XT kit with Nextera XT V2 set A indices. Samples with DNA concentrations of $>$0.2 ng/μL (43/66 samples) were diluted and normalized to 0.2 ng/μL and prepared for shotgun sequencing as described by the manufacturer. Samples with DNA concentrations of $<$0.2 ng/μL (23/66 samples) were prepared for shotgun sequencing using a "tagmentation" reaction modified and optimized for low-input samples, as described in reference 74. All indexed samples were quantified with the Qubit dsDNA HS kit, normalized, and pooled. A final, double size-selection step was performed using AMPure XP beads. Final library quality control was done using Agilent TapeStation dsDNA 5,000-bp and 1,000-bp kits. Final libraries were sequenced on an Illumina HiSeq 4000 with PE150 V3 chemistry, using two lanes, at the UC Davis DNA Technologies Core.

Viral read preprocessing. Initial quality analysis was performed with FastQC. Read preprocessing was performed by quality trimming, adapter trimming, quality filtering, and length filtering with Trimmomatic using Nextera XT adapter sequences and "palindrome" mode for adapter trimming; all other settings were defaults (75). Trimmed, paired reads were joined with PANDASeq with default parameters (76). Trimmed singletons and joined pairs were concatenated together into the final preprocessed read set for each sample.

Taxonomic read classification and abundance estimation. Overall taxonomic read classification (eukaryotic, bacterial, archaeal, and viral) was performed on preprocessed reads at the nucleotide level against the full NCBI RefSeq database with Kraken2 (40, 77). For each sample, species abundances were estimated using the Bracken package with an ideal read length of 150 bp (41). To better characterize the

viral read content, preprocessed reads were first classified against NCBI's Viral RefSeq database with Kraken2 (40, 43). The remaining, unclassified reads were reclassified against the full IMG/VR database (IMG VR 2018-07-01 4) with Kraken2 (40, 42) to minimize the occurrence of false positives (71). For each sample in each viral classification method, species/taxon abundances were estimated with Bracken using an ideal read length of 150 bp (41). Abundance reports for each sample in each viral classification method were combined into a single count table. Viral and host taxonomies were abstracted from NCBI and IMG/VR and manually curated to standardize viral species and "type"-level strings. For NCBI taxa, host association was inferred from the viral species designation, while IMG/VR host assignments were determined by a combination of viral species designation, alignment with CRISPR spacers and prophages, and deposited metadata. For taxa without a species designation, the "type" designation with a numerical identifier (ID) was used. Phage taxonomy and life cycle were inferred from IMG/VR viral cluster metadata unless otherwise specified (Table 1). After curation, NCBI and IMG/VR taxonomy tables were concatenated to create a single taxonomy table for downstream analyses.

Viral community composition and differential abundance analyses. The combined Bracken count table, taxonomy table, and a metadata mapping file were imported to RStudio and built into a phyloseq object for community composition analyses (78). Contaminants were detected and identified using Decontam, with four negative-control samples and a threshold of 0.2 (44). Additional decontamination was performed by filtering viral species, strains, and types known to be used in adjacent laboratory space; prominent contaminants are shown in Fig. S3 in the supplemental material. A large proportion of unannotated taxa remained after decontamination; unless otherwise stated, all analyses were performed with this fraction removed. No systematic difference was observed in the amounts of reads retained during decontamination for the samples having $>$0.2 ng/μL or $<$0.2 ng/μL of DNA (Fig. S9). Stacked taxonomic boxplots were generated with phyloseq after agglomeration taxa at the species or host/type level. Alpha diversity was calculated with phyloseq (78) and plotted with ggplot2 (79), and statistics were calculated with ggpubr. Beta diversity was calculated and ordinated with phyloseq; additional boxplots were made with ggplot2. All additional analyses and visualizations of community composition were performed using a combination of phyloseq, dplyr, ggplot2, and ggpubr. Differential abundance analyses were performed with DESeq2 using nonparametric fitting, the Wald test for significance, and the Benjamini-Hochberg correction for multiple hypothesis testing (80). Results were visualized with ggplot2, with error bars representing the log-fold standard error.

16S rRNA library preparation, sequencing, and bioinformatics. 16S rRNA library preparation, sequencing, and bioinformatics were performed as previously described (26, 39). Briefly, the whole-microbiome fraction was extracted by enzymatic digestion with high-activity lysozyme and proteinase K, followed by incubation with chemical lysis buffer and mechanical lysis by bead beating. Extracted DNA was purified using the PureLink genomic DNA kit, following the manufacturer's instructions. Sequencing libraries were prepared using 2-step PCR, targeting the V1-V3 loops of the 16S gene, and libraries were sequenced on an Illumina MiSeq with a PE300 kit. Reads were processed with QIIME using the open operational taxonomic unit (OTU) picking pipeline (81), and taxonomy was assigned against the SILVA128 database (82). The resulting BIOM table was imported to RStudio, along with a mapping file, and built into a phyloseq object for downstream analyses (78).

Data availability. The data sets, abundance tables, taxonomy tables, and mapping tables generated and analyzed in the present study are available in the Dryad repository (https://doi.org/10.25349/D9VG85). The R notebook used for analysis is also available in the Dryad repository (https://doi.org/10.25349/D9VG85).

SUPPLEMENTAL MATERIAL

Supplemental material is available online only.

SUPPLEMENTAL FILE 1, PDF file, 2.4 MB.

SUPPLEMENTAL FILE 2, XLSX file, 1 MB.

ACKNOWLEDGMENTS

Funding for this project was provided by the NIH New Innovator Program (grant number DP2GM123457) and the Camille Dreyfus Teacher-Scholar Program.

We thank Y. Shen for computational insights.

S.V., J.M.D., and I.A.C. designed the study. S.V. conducted experiments and performed computational analysis. J.M.D. collected patient samples. I.A.C. provided research direction. S.V. and I.A.C. wrote the manuscript with input with all authors.

We declare no competing financial or nonfinancial interests.

REFERENCES

1. Olsson M, Järbrink K, Divakar U, Bajpai R, Upton Z, Schmidtchen A, Car J. 2019. The humanistic and economic burden of chronic wounds: a systematic review. Wound Repair Regen 27:114–125. https://doi.org/10.1111/wrr.12683.
2. Martinengo L, Olsson M, Bajpai R, Soljak M, Upton Z, Schmidtchen A, Car J, Järbrink K. 2019. Prevalence of chronic wounds in the general population: systematic review and meta-analysis of observational studies. Ann Epidemiol 29:8–15. https://doi.org/10.1016/j.annepidem.2018.10.005.

3. Sen CK, Gordillo GM, Roy S, Kirsner R, Lambert L, Hunt TK, Gottrup F, Gurtner GC, Longaker MT. 2009. Human skin wounds: a major and snowballing threat to public health and the economy. Wound Repair Regen 17:763–771. https://doi.org/10.1111/j.1524-475X.2009.00543.x.
4. Loesche M, Gardner SE, Kalan L, Horwinski J, Zheng Q, Hodkinson BP, Tyldsley AS, Franciscus CL, Hillis SL, Mehta S, Margolis DJ, Grice EA. 2017. Temporal Stability in Chronic Wound Microbiota Is Associated With Poor Healing. J Invest Dermatol 137:237–244. https://doi.org/10.1016/j.jid.2016.08.009.
5. Kalan L, Loesche M, Hodkinson BP, Heilmann K, Ruthel G, Gardner SE, Grice EA. 2016. Redefining the chronic-wound microbiome: fungal communities are prevalent, dynamic, and associated with delayed healing. mBio 7:e01058-16. https://doi.org/10.1128/mBio.01058-16.
6. Kalan LR, Meisel JS, Loesche MA, Horwinski J, Soaita I, Chen X, Uberoi A, Gardner SE, Grice EA. 2019. Strain- and species-level variation in the microbiome of diabetic wounds is associated with clinical outcomes and therapeutic efficacy. Cell Host Microbe 25:641–655.e5. https://doi.org/10.1016/j.chom.2019.03.006.
7. Kalan L, Grice EA. 2018. Fungi in the wound microbiome. Adv Wound Care (New Rochelle) 7:247–255. https://doi.org/10.1089/wound.2017.0756.
8. Price LB, Liu CM, Melendez JH, Frankel YM, Engelthaler D, Aziz M, Bowers J, Rattray R, Ravel J, Kingsley C, Keim PS, Lazarus GS, Zenilman JM. 2009. Community analysis of chronic wound bacteria using 16S rRNA gene-based pyrosequencing: impact of diabetes and antibiotics on chronic wound microbiota. PLoS One 4:e6462. https://doi.org/10.1371/journal.pone.0006462.
9. Wolcott RD, Hanson JD, Rees EJ, Koenig LD, Phillips CD, Wolcott RA, Cox SB, White JS. 2016. Analysis of the chronic wound microbiota of 2,963 patients by 16S rDNA pyrosequencing. Wound Repair Regen 24:163–174. https://doi.org/10.1111/wrr.12370.
10. Gardiner M, Vicaretti M, Sparks J, Bansal S, Bush S, Liu M, Darling A, Harry E, Burke CM. 2017. A longitudinal study of the diabetic skin and wound microbiome. PeerJ 5:e3543. https://doi.org/10.7717/peerj.3543.
11. Dowd SE, Sun Y, Secor PR, Rhoads DD, Wolcott BM, James GA, Wolcott RD. 2008. Survey of bacterial diversity in chronic wounds using pyrosequencing, DGGE, and full ribosome shotgun sequencing. BMC Microbiol 8:43. https://doi.org/10.1186/1471-2180-8-43.
12. Scales BS, Huffnagle GB. 2013. The microbiome in wound repair and tissue fibrosis. J Pathol 229:323–331. https://doi.org/10.1002/path.4118.
13. Sanchez-Sanchez M, Cruz-Pulido WL, Bladinieres-Cámara E, Alcalá-Durán R, Rivera-Sánchez G, Bocanegra-García V. 2017. Bacterial prevalence and antibiotic resistance in clinical isolates of diabetic foot ulcers in the northeast of Tamaulipas, Mexico. Int J Low Extrem Wounds 16:129–134. https://doi.org/10.1177/1534734617705254.
14. Rahim K, Saleha S, Zhu X, Huo L, Basit A, Franco OL. 2017. Bacterial contribution in chronicity of wounds. Microb Ecol 73:710–721. https://doi.org/10.1007/s00248-016-0867-9.
15. Price LB, Liu CM, Frankel YM, Melendez JH, Aziz M, Buchhagen J, Contente-Cuomo T, Engelthaler DM, Keim PS, Ravel J, Lazarus GS, Zenilman JM. 2011. Macroscale spatial variation in chronic wound microbiota: a cross-sectional study. Wound Repair Regen 19:80–88. https://doi.org/10.1111/j.1524-475X.2010.00628.x.
16. Phalak P, Henson MA. 2019. Metabolic modelling of chronic wound microbiota predicts mutualistic interactions that drive community composition. J Appl Microbiol 127:1576–1593. https://doi.org/10.1111/jam.14421.
17. Liu S-H, Huang Y-C, Chen LY, Yu S-C, Yu H-Y, Chuang S-S. 2018. The skin microbiome of wound scars and unaffected skin in patients with moderate to severe burns in the subacute phase. Wound Repair Regen 26:182–191. https://doi.org/10.1111/wrr.12632.
18. Johnson TR, Gómez BI, McIntyre MK, Dubick MA, Christy RJ, Nicholson SE, Burmeister DM. 2018. The cutaneous microbiome and wounds: new molecular targets to promote wound healing. Int J Mol Sci 19:2699. https://doi.org/10.3390/ijms19092699.
19. Jneid J, Cassir N, Schuldiner S, Jourdan N, Sotto A, Lavigne J-P, La Scola B. 2018. Exploring the microbiota of diabetic foot infections with culturomics. Front Cell Infect Microbiol 8:282. https://doi.org/10.3389/fcimb.2018.00282.
20. Holmes CJ, Plichta JK, Gamelli RL, Radek KA. 2015. Dynamic role of host stress responses in modulating the cutaneous microbiome: implications for wound healing and infection. Adv Wound Care (New Rochelle) 4:24–37. https://doi.org/10.1089/wound.2014.0546.
21. Halstead FD, Lee KC, Kwei J, Dretzke J, Oppenheim BA, Moiemen NS. 2018. A systematic review of quantitative burn wound microbiology in the management of burns patients. Burns 44:39–56. https://doi.org/10.1016/j.burns.2017.06.008.
22. Grice EA, Snitkin ES, Yockey LJ, Bermudez DM, Liechty KW, Segre JA, NISC Comparative Sequencing Program. 2010. Longitudinal shift in diabetic wound microbiota correlates with prolonged skin defense response. Proc Natl Acad Sci U S A 107:14799–14804. https://doi.org/10.1073/pnas.1004204107.
23. Gjodsbol K, Skindersoe ME, Christensen JJ, Karlsmark T, Jørgensen B, Jensen AM, Klein BM, Sonnested MK, Krogfelt KA. 2012. No need for biopsies: comparison of three sample techniques for wound microbiota determination. Int Wound J 9:295–302. https://doi.org/10.1111/j.1742-481X.2011.00883.x.
24. Canesso MCC, Vieira AT, Castro TBR, Schirmer BGA, Cisalpino D, Martins FS, Rachid MA, Nicoli JR, Teixeira MM, Barcelos LS. 2014. Skin wound healing is accelerated and scarless in the absence of commensal microbiota. J Immunol 193:5171–5180. https://doi.org/10.4049/jimmunol.1400625.
25. Ammons MCB, Morrissey K, Tripet BP, Van Leuven JT, Han A, Lazarus GS, Zenilman JM, Stewart PS, James GA, Copié V. 2015. Biochemical association of metabolic profile and microbiome in chronic pressure ulcer wounds. PLoS One 10:e0126735. https://doi.org/10.1371/journal.pone.0126735.
26. Verbanic S, Shen Y, Lee J, Deacon JM, Chen IA. 2020. Microbial predictors of healing and short-term effect of debridement on the microbiome of chronic wounds. NPJ Biofilms Microbiomes 6:21. https://doi.org/10.1038/s41522-020-0130-5.
27. Zarate S, Taboada B, Yocupicio-Monroy M, Arias CF. 2017. Human virome. Arch Med Res 48:701–716. https://doi.org/10.1016/j.arcmed.2018.01.005.
28. Norman JM, Handley SA, Baldridge MT, Droit L, Liu CY, Keller BC, Kambal A, Monaco CL, Zhao G, Fleshner P, Stappenbeck TS, McGovern DPB, Keshavarzian A, Mutlu EA, Sauk J, Gevers D, Xavier RJ, Wang D, Parkes M, Virgin HW. 2015. Disease-specific alterations in the enteric virome in inflammatory bowel disease. Cell 160:447–460. https://doi.org/10.1016/j.cell.2015.01.002.
29. Keen EC. 2015. A century of phage research: bacteriophages and the shaping of modern biology. Bioessays 37:6–9. https://doi.org/10.1002/bies.201400152.
30. Clokie MR, Millard AD, Letarov AV, Heaphy S. 2011. Phages in nature. Bacteriophage 1:31–45. https://doi.org/10.4161/bact.1.1.14942.
31. Howard-Varona C, Hargreaves KR, Abedon ST, Sullivan MB. 2017. Lysogeny in nature: mechanisms, impact and ecology of temperate phages. ISME J 11:1511–1520. https://doi.org/10.1038/ismej.2017.16.
32. Secor PR, Michaels LA, Smigiel KS, Rohani MG, Jennings LK, Hisert KB, Arrigoni A, Braun KR, Birkland TP, Lai Y, Hallstrand TS, Bollyky PL, Singh PK, Parks WC. 2017. Filamentous bacteriophage produced by *Pseudomonas aeruginosa* alters the inflammatory response and promotes noninvasive infection *in vivo*. Infect Immun 85:e00648-16. https://doi.org/10.1128/IAI.00648-16.
33. Barr JJ, Auro R, Furlan M, Whiteson KL, Erb ML, Pogliano J, Stotland A, Wolkowicz R, Cutting AS, Doran KS, Salamon P, Youle M, Rohwer F. 2013. Bacteriophage adhering to mucus provide a non-host-derived immunity. Proc Natl Acad Sci U S A 110:10771–10776. https://doi.org/10.1073/pnas.1305923110.
34. Gomaa S, Serry F, Abdellatif H, Abbas H. 2019. Elimination of multidrug-resistant *Proteus mirabilis* biofilms using bacteriophages. Arch Virol 164:2265–2275. https://doi.org/10.1007/s00705-019-04305-x.
35. Oh J, Byrd AL, Park M, Kong HH, Segre JA, NISC Comparative Sequencing Program. 2016. Temporal stability of the human skin microbiome. Cell 165:854–866. https://doi.org/10.1016/j.cell.2016.04.008.
36. Foulongne V, Sauvage V, Hebert C, Dereure O, Cheval J, Gouilh MA, Pariente K, Segondy M, Burguière A, Manuguerra J-C, Caro V, Eloit M. 2012. Human skin microbiota: high diversity of DNA viruses identified on the human skin by high throughput sequencing. PLoS One 7:e38499. https://doi.org/10.1371/journal.pone.0038499.
37. Hannigan GD, Meisel JS, Tyldsley AS, Zheng Q, Hodkinson BP, SanMiguel AJ, Minot S, Bushman FD, Grice EA. 2015. The human skin double-stranded DNA virome: topographical and temporal diversity, genetic enrichment, and dynamic associations with the host microbiome. mBio 6:e01578-15. https://doi.org/10.1128/mBio.01578-15.
38. Garmaeva S, Sinha T, Kurilshikov A, Fu J, Wijmenga C, Zhernakova A. 2019. Studying the gut virome in the metagenomic era: challenges and perspectives. BMC Biol 17:84. https://doi.org/10.1186/s12915-019-0704-y.
39. Verbanic S, Kim CY, Deacon JM, Chen IA. 2019. Improved single-swab sample preparation for recovering bacterial and phage DNA from human skin and wound microbiomes. BMC Microbiol 19:214. https://doi.org/10.1186/s12866-019-1586-4.

40. Wood DE, Lu J, Langmead B. 2019. Improved metagenomic analysis with Kraken 2. Genome Biol 20:257. https://doi.org/10.1186/s13059-019-1891-0.
41. Lu J, Breitwieser FP, Thielen P, Salzberg SL. 2017. Bracken: estimating species abundance in metagenomics data. PeerJ Comput Sci 3:e104. https://doi.org/10.7717/peerj-cs.104.
42. Paez-Espino D, Chen I-MA, Palaniappan K, Ratner A, Chu K, Szeto E, Pillay M, Huang J, Markowitz VM, Nielsen T, Huntemann M, Reddy TBK, Pavlopoulos GA, Sullivan MB, Campbell BJ, Chen F, McMahon K, Hallam SJ, Denef V, Cavicchioli R, Caffrey SM, Streit WR, Webster J, Handley KM, Salekdeh GH, Tsesmetzis N, Setubal JC, Pope PB, Liu W-T, Rivers AR, Ivanova NN, Kyrpides NC. 2017. IMG/VR: a database of cultured and uncultured DNA viruses and retroviruses. Nucleic Acids Res 45:D457–D465. https://doi.org/10.1093/nar/gkw1030.
43. Brister JR, Ako-Adjei D, Bao Y, Blinkova O. 2015. NCBI viral genomes resource. Nucleic Acids Res 43:D571–D577. https://doi.org/10.1093/nar/gku1207.
44. Davis NM, Proctor DM, Holmes SP, Relman DA, Callahan BJ. 2018. Simple statistical identification and removal of contaminant sequences in marker-gene and metagenomics data. Microbiome 6:226. https://doi.org/10.1186/s40168-018-0605-2.
45. Roux S, Enault F, Hurwitz BL, Sullivan MB. 2015. VirSorter: mining viral signal from microbial genomic data. PeerJ 3:e985. https://doi.org/10.7717/peerj.985.
46. Roux S, Hallam SJ, Woyke T, Sullivan MB. 2015. Viral dark matter and virus-host interactions resolved from publicly available microbial genomes. Elife 4:e08490. https://doi.org/10.7554/eLife.08490.
47. Krishnamurthy SR, Wang D. 2017. Origins and challenges of viral dark matter. Virus Res 239:136–142. https://doi.org/10.1016/j.virusres.2017.02.002.
48. Zhao G, Wu G, Lim ES, Droit L, Krishnamurthy S, Barouch DH, Virgin HW, Wang D. 2017. VirusSeeker, a computational pipeline for virus discovery and virome composition analysis. Virology 503:21–30. https://doi.org/10.1016/j.virol.2017.01.005.
49. Ren J, Ahlgren NA, Lu YY, Fuhrman JA, Sun F. 2017. VirFinder: a novel k-mer based tool for identifying viral sequences from assembled metagenomic data. Microbiome 5:69. https://doi.org/10.1186/s40168-017-0283-5.
50. Roux S, Tournayre J, Mahul A, Debroas D, Enault F. 2014. Metavir 2: new tools for viral metagenome comparison and assembled virome analysis. BMC Bioinformatics 15:76. https://doi.org/10.1186/1471-2105-15-76.
51. Naccache SN, Federman S, Veeraraghavan N, Zaharia M, Lee D, Samayoa E, Bouquet J, Greninger AL, Luk K-C, Enge B, Wadford DA, Messenger SL, Genrich GL, Pellegrino K, Grard G, Leroy E, Schneider BS, Fair JN, Martínez MA, Isa P, Crump JA, DeRisi JL, Sittler T, Hackett J, Miller S, Chiu CY. 2014. A cloud-compatible bioinformatics pipeline for ultrarapid pathogen identification from next-generation sequencing of clinical samples. Genome Res 24:1180–1192. https://doi.org/10.1101/gr.171934.113.
52. Paez-Espino D, Pavlopoulos GA, Ivanova NN, Kyrpides NC. 2017. Nontargeted virus sequence discovery pipeline and virus clustering for metagenomic data. Nat Protoc 12:1673–1682. https://doi.org/10.1038/nprot.2017.063.
53. Lopez E, Domenech A, Ferrándiz MJ, Frias MJ, Ardanuy C, Ramirez M, García E, Liñares J, de la Campa AG. 2014. Induction of prophages by fluoroquinolones in Streptococcus pneumoniae: implications for emergence of resistance in genetically-related clones. PLoS One 9:e94358. https://doi.org/10.1371/journal.pone.0094358.
54. Wagner PL, Neely MN, Zhang X, Acheson DW, Waldor MK, Friedman DI. 2001. Role for a phage promoter in Shiga toxin 2 expression from a pathogenic *Escherichia coli* strain. J Bacteriol 183:2081–2085. https://doi.org/10.1128/JB.183.6.2081-2085.2001.
55. Nanda AM, Heyer A, Krämer C, Grünberger A, Kohlheyer D, Frunzke J. 2014. Analysis of SOS-induced spontaneous prophage induction in *Corynebacterium glutamicum* at the single-cell level. J Bacteriol 196:180–188. https://doi.org/10.1128/JB.01018-13.
56. Choi JD, Kotay SM, Goel R. 2010. Various physico-chemical stress factors cause prophage induction in *Nitrosospira multiformis* 25196-an ammonia oxidizing bacteria. Water Res 44:4550–4558. https://doi.org/10.1016/j.watres.2010.04.040.
57. Nanda AM, Thormann K, Frunzke J. 2015. Impact of spontaneous prophage induction on the fitness of bacterial populations and host-microbe interactions. J Bacteriol 197:410–419. https://doi.org/10.1128/JB.02230-14.
58. Mariem BJ-J, Ito T, Zhang M, Jin J, Li S, Ilhem B-BB, Adnan H, Han X, Hiramatsu K. 2013. Molecular characterization of methicillin-resistant Panton-Valentine leukocidin positive *Staphylococcus aureus* clones disseminating in Tunisian hospitals and in the community. BMC Microbiol 13:2. https://doi.org/10.1186/1471-2180-13-2.
59. Kaneko J, Narita-Yamada S, Wakabayashi Y, Kamio Y. 2009. Identification of ORF636 in phage phi SLT carrying Panton-Valentine leukocidin genes, acting as an adhesion protein for a poly(glycerophosphate) chain of lipoteichoic acid on the cell surface of *Staphylococcus aureus*. J Bacteriol 191:4674–4680. https://doi.org/10.1128/JB.01793-08.
60. Obeng N, Pratama AA, van Elsas JD. 2016. The significance of mutualistic phages for bacterial ecology and evolution. Trends Microbiol 24:440–449. https://doi.org/10.1016/j.tim.2015.12.009.
61. Tsao Y-F, Taylor VL, Kala S, Bondy-Denomy J, Khan AN, Bona D, Cattoir V, Lory S, Davidson AR, Maxwell KL. 2018. Phage morons play an important role in *Pseudomonas aeruginosa* phenotypes. J Bacteriol 200:e00189-18. https://doi.org/10.1128/JB.00189-18.
62. Zegans ME, Wagner JC, Cady KC, Murphy DM, Hammond JH, O'Toole GA. 2009. Interaction between bacteriophage DMS3 and host CRISPR region inhibits group behaviors of *Pseudomonas aeruginosa*. J Bacteriol 191:210–219. https://doi.org/10.1128/JB.00797-08.
63. Bondy-Denomy J, Pawluk A, Maxwell KL, Davidson AR. 2013. Bacteriophage genes that inactivate the CRISPR/Cas bacterial immune system. Nature 493:429–432. https://doi.org/10.1038/nature11723.
64. Gutierrez D, Martínez B, Rodríguez A, García P. 2012. Genomic characterization of two *Staphylococcus epidermidis* bacteriophages with anti-biofilm potential. BMC Genomics 13:228. https://doi.org/10.1186/1471-2164-13-228.
65. Chan BK, Abedon ST. 2015. Bacteriophages and their enzymes in biofilm control. Curr Pharm Des 21:85–99. https://doi.org/10.2174/1381612820666140905112311.
66. Fan X, Li W, Zheng F, Xie J. 2013. Bacteriophage inspired antibiotics discovery against infection involved biofilm. Crit Rev Eukaryot Gene Expr 23:317–326. https://doi.org/10.1615/critreveukaryotgeneexpr.2013007717.
67. Sillankorva S, Azeredo J. 2014. The use of bacteriophages and bacteriophage-derived enzymes for clinically relevant biofilm control, p 309–329. *In* Borysowski J, Międzybrodzki R, Górski A (ed), Phage therapy: current research and applications. Caister Academic Press, Poole, United Kingdom.
68. Borges AL, Zhang JY, Rollins MF, Osuna BA, Wiedenheft B, Bondy-Denomy J. 2018. Bacteriophage cooperation suppresses CRISPR-Cas3 and Cas9 immunity. Cell 174:917–925.e10. https://doi.org/10.1016/j.cell.2018.06.013.
69. Dunyach-Remy C, Ngba Essebe C, Sotto A, Lavigne J-P. 2016. *Staphylococcus aureus* toxins and diabetic foot ulcers: role in pathogenesis and interest in diagnosis. Toxins (Basel) 8:209. https://doi.org/10.3390/toxins8070209.
70. Yazdi M, Bouzari M, Ghaemi EA. 2018. Isolation and characterization of a lytic bacteriophage (vB_PmiS-TH) and its application in combination with ampicillin against planktonic and biofilm forms of *Proteus mirabilis* isolated from urinary tract infection. J Mol Microbiol Biotechnol 28:37–46. https://doi.org/10.1159/000487137.
71. Glickman C, Hendrix J, Strong M. 2021. Simulation study and comparative evaluation of viral contiguous sequence identification tools. BMC Bioinformatics 22:329. https://doi.org/10.1186/s12859-021-04242-0.
72. Eisenhofer R, Minich JJ, Marotz C, Cooper A, Knight R, Weyrich LS. 2019. Contamination in low microbial biomass microbiome studies: issues and recommendations. Trends Microbiol 27:105–117. https://doi.org/10.1016/j.tim.2018.11.003.
73. Salter SJ, Cox MJ, Turek EM, Calus ST, Cookson WO, Moffatt MF, Turner P, Parkhill J, Loman NJ, Walker AW. 2014. Reagent and laboratory contamination can critically impact sequence-based microbiome analyses. BMC Biol 12:87. https://doi.org/10.1186/s12915-014-0087-z.
74. Rinke C, Low S, Woodcroft BJ, Raina J-B, Skarshewski A, Le XH, Butler MK, Stocker R, Seymour J, Tyson GW, Hugenholtz P. 2016. Validation of picogram- and femtogram-input DNA libraries for microscale metagenomics. PeerJ 4:e2486. https://doi.org/10.7717/peerj.2486.
75. Bolger AM, Lohse M, Usadel B. 2014. Trimmomatic: a flexible trimmer for Illumina sequence data. Bioinformatics 30:2114–2120. https://doi.org/10.1093/bioinformatics/btu170.
76. Masella AP, Bartram AK, Truszkowski JM, Brown DG, Neufeld JD. 2012. PANDAseq: PAired-eND Assembler for Illumina sequences. BMC Bioinformatics 13:31. https://doi.org/10.1186/1471-2105-13-31.
77. O'Leary NA, Wright MW, Brister JR, Ciufo S, Haddad D, McVeigh R, Rajput B, Robbertse B, Smith-White B, Ako-Adjei D, Astashyn A, Badretdin A, Bao Y, Blinkova O, Brover V, Chetvernin V, Choi J, Cox E, Ermolaeva O, Farrell CM, Goldfarb T, Gupta T, Haft D, Hatcher E, Hlavina W, Joardar VS, Kodali VK, Li W, Maglott D, Masterson P, McGarvey KM, Murphy MR, O'Neill K, Pujar S, Rangwala SH, Rausch D, Riddick LD, Schoch C, Shkeda A, Storz SS, Sun H, Thibaud-Nissen F, Tolstoy I, Tully RE, Vatsan AR, Wallin C, Webb D, Wu W, Landrum MJ, Kimchi A, Tatusova T, DiCuccio M, Kitts P, Murphy TD, Pruitt KD. 2016. Reference sequence (RefSeq) database at NCBI: current

status, taxonomic expansion, and functional annotation. Nucleic Acids Res 44:D733–D745. https://doi.org/10.1093/nar/gkv1189.
78. McMurdie PJ, Holmes S. 2013. phyloseq: an R package for reproducible interactive analysis and graphics of microbiome census data. PLoS One 8: e61217. https://doi.org/10.1371/journal.pone.0061217.
79. Wickham H. 2009. ggplot2: elegant graphics for data analysis. Springer, New York, NY USA.
80. Love MI, Huber W, Anders S. 2014. Moderated estimation of fold change and dispersion for RNA-seq data with DESeq2. Genome Biol 15:550. https://doi.org/10.1186/s13059-014-0550-8.
81. Caporaso JG, Kuczynski J, Stombaugh J, Bittinger K, Bushman FD, Costello EK, Fierer N, Peña AG, Goodrich JK, Gordon JI, Huttley GA, Kelley ST, Knights D, Koenig JE, Ley RE, Lozupone CA, McDonald D, Muegge BD, Pirrung M, Reeder J, Sevinsky JR, Turnbaugh PJ, Walters WA, Widmann J, Yatsunenko T, Zaneveld J, Knight R. 2010. QIIME allows analysis of high-throughput community sequencing data. Nat Methods 7:335–336. https://doi.org/10.1038/nmeth.f.303.
82. Quast C, Pruesse E, Yilmaz P, Gerken J, Schweer T, Yarza P, Peplies J, Glöckner FO. 2013. The SILVA ribosomal RNA gene database project: improved data processing and web-based tools. Nucleic Acids Res 41: D590–D596. https://doi.org/10.1093/nar/gks1219.
83. Villafane R, Zayas M, Gilcrease EB, Kropinski AM, Casjens SR. 2008. Genomic analysis of bacteriophage epsilon 34 of *Salmonella enterica* serovar Anatum (15+). BMC Microbiol 8:227. https://doi.org/10.1186/1471-2180-8-227.
84. Depardieu F, Didier J-P, Bernheim A, Sherlock A, Molina H, Duclos B, Bikard D. 2016. A eukaryotic-like serine/threonine kinase protects staphylococci against phages. Cell Host Microbe 20:471–481. https://doi.org/10.1016/j.chom.2016.08.010.
85. Deghorain M, Bobay L-M, Smeesters PR, Bousbata S, Vermeersch M, Perez-Morga D, Drèze P-A, Rocha EPC, Touchon M, Van Melderen L. 2012. Characterization of novel phages isolated in coagulase-negative staphylococci reveals evolutionary relationships with *Staphylococcus aureus* phages. J Bacteriol 194:5829–5839. https://doi.org/10.1128/JB.01085-12.
86. Daniel A, Bonnen PE, Fischetti VA. 2007. First complete genome sequence of two *Staphylococcus epidermidis* bacteriophages. J Bacteriol 189: 2086–2100. https://doi.org/10.1128/JB.01637-06.
87. Barylski J, Kropinski AM, Alikhan NF, Adriaenssens EM, ICTV Report Consortium. 2020. ICTV virus taxonomy profile: *Herelleviridae*. J Gen Virol 101: 362–363. https://doi.org/10.1099/jgv.0.001392.
88. Iandolo JJ, Worrell V, Groicher KH, Qian Y, Tian R, Kenton S, Dorman A, Ji H, Lin S, Loh P, Qi S, Zhu H, Roe BA. 2002. Comparative analysis of the genomes of the temperate bacteriophages phi 11, phi 12 and phi 13 of *Staphylococcus aureus* 8325. Gene 289:109–118. https://doi.org/10.1016/S0378-1119(02)00481-X.
89. Adriaenssens EM, Wittmann J, Kuhn JH, Turner D, Sullivan MB, Dutilh BE, Jang HB, van Zyl LJ, Klumpp J, Lobocka M, Moreno Switt AI, Rumnieks J, Edwards RA, Uchiyama J, Alfenas-Zerbini P, Petty NK, Kropinski AM, Barylski J, Gillis A, Clokie MRC, Prangishvili D, Lavigne R, Aziz RK, Duffy S, Krupovic M, Poranen MM, Knezevic P, Enault F, Tong Y, Oksanen HM, Rodney Brister J. 2018. Taxonomy of prokaryotic viruses: 2017 update from the ICTV Bacterial and Archaeal Viruses Subcommittee. Arch Virol 163:1125–1129. https://doi.org/10.1007/s00705-018-3723-z.
90. Cheng S, Xing S, Zhang X, Pei G, An X, Mi Z, Huang Y, Tong Y. 2016. Complete genome sequence of a new *Enterococcus faecalis* bacteriophage, vB_EfaS_IME197. Genome Announc 4:e00827-16. https://doi.org/10.1128/genomeA.00827-16.
91. Mohamed DH, Saberesheikh S, Kearns AM, Saunders NA. 2012. Putative link between *Staphylococcus aureus* bacteriophage serotype and community association. Int J Med Microbiol 302:135–144. https://doi.org/10.1016/j.ijmm.2012.02.002.
92. Deghorain M, Van Melderen L. 2012. The staphylococci phages family: an overview. Viruses 4:3316–3335. https://doi.org/10.3390/v4123316.
93. Nelson D, Schuch R, Zhu S, Tscherne DM, Fischetti VA. 2003. Genomic sequence of C1, the first streptococcal phage. J Bacteriol 185:3325–3332. https://doi.org/10.1128/JB.185.11.3325-3332.2003.